CENTENARY LECTURE

Rotationally and Vibrationally Inelastic Scattering of Molecules

By J. P. Toennies
MAX-PLANCK-INSTITUT FÜR STRÖMUNGSFORSCHUNG,
34 GÖTTINGEN, GERMANY

1 Introduction

Vibrationally and rotationally inelastic scattering are the simplest of the energy-transfer collision processes. They are of great importance for understanding the kinetics of gas-phase chemical reactions, energy balance in plasmas and astrophysical systems, relaxation phenomena in fast-flow phenomena such as shock waves and nozzle expansions, as well as in numerous other non-equilibrium systems. Energy-transfer collisions also influence the rate of radiation and thus determine the broadening and shift of spectral lines and the population and de-population of excited states. A technological device in which energy-transfer processes play an important role is the gas-phase laser.

Inelastic collisions have an intermediate position in the hierarchy of bimolecular collision processes. The simpler *elastic* collisions, involving only changes in the direction and magnitudes of the translational velocity of the scattered particles with respect to their centre of mass, are now so well understood that they are routinely used in molecular-beam scattering experiments for the measurement of the van der Waals potential-energy curves between two atoms. On the other hand, the more complex *reactive* collisions in which, in addition to changes in velocities (as in *elastic* collisions) and in internal states (as in *inelastic* collisions), there are changes in chemical species and structure, still present formidable fundamental theoretical problems.

In this review we will deal with the simplest of all inelastic collision processes:

$$\mathrm{A} + \mathrm{BC}(j_\mathrm{i}, n_\mathrm{i}) \rightarrow \mathrm{A} + \mathrm{BC}(j_\mathrm{f}, n_\mathrm{f}) \pm \Delta E_\mathrm{trans} \qquad (1)$$

where A, B, and C are atoms or ions, and j and n are the rotational and vibrational quantum numbers, respectively, and the index i denotes the initial state and f the final state. ΔE_trans denotes the change in relative translational energy. Within the past few years it has become possible to calculate the potential hypersurface and the quantum-mechanical inelastic cross-sections for a number of systems having a few electrons. We will therefore direct our attention to recent beam-scattering experiments on such systems for which a detailed comparison between theory and experiment is possible. As we shall see, these studies provide deep insight into the dynamical features of molecular collisions and should

eventually prove useful for understanding the more complicated reactive collisions.

A. Bulk Energy Transfer in the Gas Phase.—Despite the recent successes of beam-scattering experiments, most of our information on energy transfer comes from bulk studies.[1] This has had a profound influence on the theoretical methods developed for describing energy transfer.[2] For this reason, and because the results of beam studies will hopefully contribute to a better understanding of bulk energy transfer, we begin by briefly surveying the bulk studies.

If we restrict ourselves to the gas phase we can broadly classify the bulk methods into the following two groups:

(1) Relaxation studies (*e.g.* absorption and dispersion of sound, shock-front thickness measurements, expansion flow studies, spectrophone, *etc.*). In all these studies a sample of gas is suddenly subjected to a change in thermal translational energy. This energy then passes into the internal degrees of freedom until a new equilibrium state with temperature T is reached. One usually observes the resulting time variation in some bulk property or in the population of some quantum state (*e.g.* by spectroscopic emission or absorption studies). The rate of change of this property y is usually well described by a rate equation of the form:[3]

$$\frac{dy}{dt} = \frac{1}{\tau}[y - y_{eq}(T)] \tag{2}$$

where τ is the relaxation time. For the simplest case of a two-level system, τ is related to the forward and backward rate constants by

$$\frac{1}{\tau} = n_{tot}(k_{\rightarrow} + k_{\leftarrow}) \tag{3}$$

where n_{tot} is the total density of molecules.

(2) Static spectroscopic studies (*e.g.* microwave line broadening, line shift, and fluorescence studies). Here some spectral feature is measured under static conditions as a function of pressure. Information on relative rate constants results since the radiating states have a natural lifetime which may be shortened by the occurrence of inelastic collisions. In the case of the closely spaced microwave lines the lifetime shortening is observed directly as a pressure-dependent broadening of the spectral line. In laser fluorescence studies a molecule is first formed in a specified internal quantum state of some electronically excited

[1] For recent reviews of bulk studies see (*a*) A. B. Callear and J. D. Lambert, in vol. 3 of 'Comprehensive Chemical Kinetics' ed. C. H Bamford and C. F. H. Tipper, Elsevier, Amsterdam, 1969, p. 182; (*b*) B. Stevens, 'Collisional Activation of Gases', Pergamon Press, London, 1967; (*c*) 'Transfer and Storage of Energy by Molecules', ed. G. M. Barnett and A. M. North, Vol. 2, 'Vibrational Energy Transfer', Wiley – Interscience, London, 1969; (*d*) C. B. Moore, *Adv. Chem. Phys.*, 1973, **23**, 41.

[2] D. Rapp and T. Kassal, *Chem. Rev.*, 1969, **69**, 61.

[3] K. F. Herzfeld and T. A. Litovitz, 'Absorption and Dispersion of Ultrasonic Waves', Academic Press, New York, 1969.

state.[4] If, during its short radiative lifetime ($\approx 10^{-8}$ s), the molecule undergoes an inelastic collision to another internal state, a new line emanating from this state appears. Thus the steady-state concentration of molecules in the new state n_f, which is proportional to the associated line strength, is given by

$$n_f = n_i \, k_{i \to f} \, \tau_{eff} \, n_{tot} \tag{4}$$

where τ_{eff} is an effective radiative lifetime of the excited state and n_{tot} is the total density, which is determined by the diluent gas with which the excited molecules collide ($n_{tot} \gg n_i$).

Thus in both cases a rate constant is measured. If, as is commonly the case in spectroscopic studies and sometimes in relaxation studies, only two internal states i and f are involved, then the measured rate constants can be directly related to the collision cross-sections describing the outcome of a single collision by the following expression:

$$k_{i \to f}(T) = \int_{v_A} \int_{v_{BC}} \sigma^{i \to f}(g) \, g \, f_A(v_A, T) \, f_{BC}(v_{BC}, T) \, d\vec{v}_A \, d\vec{v}_{BC} \tag{5}$$

where g is the relative velocity ($\vec{g} = \vec{v}_A - \vec{v}_{BC}$) and $f_A(v_A, T)$ and $f_{BC}(v_{BC}, T)$ are the velocity-distribution functions.[5] $\sigma^{i \to f}(g)$ is called the integral cross-section. It is related to the differential cross-section $d^2\sigma/d^2\omega(g; \vartheta, \phi)$, which gives the probability that particles with a velocity g are inelastically scattered through the centre-of-mass angles ϑ and ϕ by:

$$\sigma^{i \to f}(g) = \int_{\vartheta} \int_{\phi} \frac{d^2\sigma}{d^2\omega}^{i \to f}(g; \vartheta, \phi) \sin \vartheta \, d\vartheta \, d\phi \, .$$

We shall say more about the differential cross-section in the next section. For present purposes it is important to realize that in the most favourable case the measured rate constants obtained in bulk experiments are averages over the relative velocity dependence of the integral cross-section, which in turn is the integral over the angle dependence of the differential cross-section. Thus many of the detailed features of the collision process are smeared over and cannot be determined from bulk studies. Such detailed knowledge is needed, for example, to predict bulk rates at temperatures outside the experimentally accessible range (*e.g.* shock waves, nozzle beam expansions *etc.*).

B. Theoretical Description of Inelastic Collisions.—Theory provides another possible approach that in principle does not suffer from the difficulties discussed above. The theoretical steps involved in an *a priori* calculation of rate constants are summarized on the left-hand side of Figure 1. As always, quantum theory

[4] For a recent review see (*a*) G. Ennen and Ch. Ottinger, *Chem. Phys.*, 1974, **3**, 404; (*b*) J. I. Steinfeld in 'Molecular Spectroscopy: Modern Research', ed. K. N. Rao and C. W. Mathews, Academic Press, New York, 1972, p. 223 ff.

[5] K. Shuler, J. Ross, and J. Light, in 'Kinetic Processes in Gases and Plasmas', ed. A. R. Hochstim, Academic Press, New York, 1969.

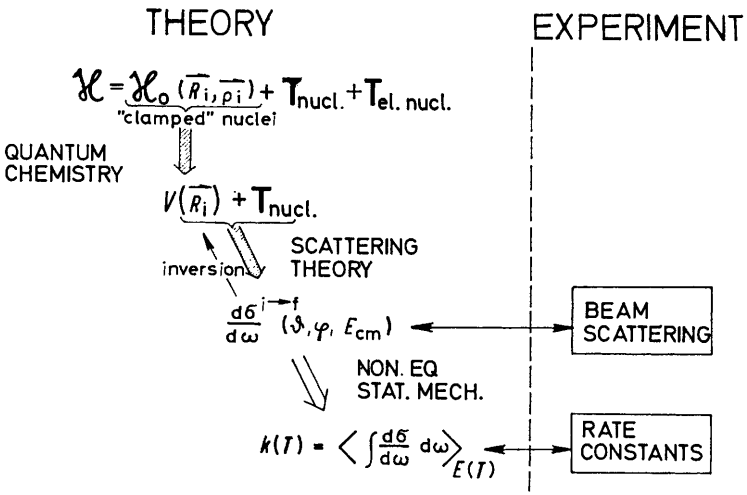

Figure 1 *Schematic diagram showing on the left the main steps in the* ab initio *theoretical calculation of rate constants. The arrows indicate the direction in which the calculations can be carried out. The experimental contributions are indicated at the right*

starts with the Hamilton operator. For the general collision problem the Hamilton operator consists of a term $\mathcal{H}_0$ containing the kinetic energy of all the electrons as well as the coulomb potential between all the electrons and nuclei. Then follows a term describing the kinetic energy of the nuclei, and finally a term which couples the wavefunctions of the nuclei to that of the electrons. The solution of the Schrödinger equation only becomes feasible if one neglects this last term. This is the essential assumption in the well-known Born–Oppenheimer approximation, which leads to a separation of the problem into two steps.[6]

In the first step one calculates the total eigen-energy of the system with the nuclei clamped in a given configuration with respect to each other, using standard quantum chemical methods. These calculations are then repeated for the range of relative configurations of interest for the particular scattering problem. In this way a potential-energy surface is generated, which, since it depends on at least three co-ordinates (see Figure 3), is called a potential hypersurface. This provides a complete description of the forces on the particles during the collision in the approximation outlined above.

In the second step the potential-energy hypersurface is used with the nuclear kinetic energy operator to set up the scattering problem. Essentially, two approximate methods have been used to solve the scattering problem, *viz.*

[6] For a discussion of the Born–Oppenheimer and the slightly more accurate Born and adiabatic approximations see (*a*) V. K. Deshpande and J. Mahauty, *Amer. J. Phys.*, 1969, **37**, 823; (*b*) E. Teller and H. L. Sahlin in 'Physical Chemistry, An Advanced Treatise', Vol. V, ed. H. Eyring, D. Henderson, and W. Jost, Academic Press, New York, 1970, p. 1 ff.; (*c*) W. Kolos and L. Wolniewicz, *Rev. Mod. Phys.*, 1963, **35**, 473.

classical mechanics and an approximate quantum-mechanical formalism. In the classical approximation the assumption is made that the motion is classical throughout the collision. The final quantum states are determined by arbitrarily partitioning the continuum of final classical states into 'boxes' and attributing the number of events in each 'box' to a quantum state. The validity of this approximation can only be tested by comparison with either more accurate quantum-mechanical scattering calculations or with experiment. The accuracy of the usual quantum-mechanical formalism is limited by the size of the basis set, which is always restricted to a finite number of terms. The final result of the scattering calculation is the differential cross-section for all scattering angles, which can be compared directly with experiment.

The result of a nearly exact quantum-mechanical scattering calculation for the scattering of a helium atom on a para-hydrogen molecule ($j = 0$) at 1.09 eV relative energy is shown in Figure 2.[7] The elastic cross-section ($j = 0 \rightarrow j = 0$) and the inelastic cross-section for rotational excitation ($j = 0 \rightarrow j = 2$) are plotted to the scale shown at the left. The potential is based on the quantum chemical calculations of Gordon and Secrest,[8] with a modification of the long-range part to bring it into agreement with elastic scattering experiments. The basis set included the following 8 states: $n = 0$, with $j = 0$, 2, 4, and 6, and $n = 1$ with $j = 0$, 2, 4, and 6.

The elastic cross-section in Figure 2 shows the typical behaviour observed in the elastic scattering of two atoms, with a sharp maximum at $\vartheta = 0°$. The inelastic cross-section for pure vibrational excitation and coupled vibrational and rotational excitation is plotted to the scale shown at the right. These cross-sections are smaller by four orders of magnitude and are peaked in the backwards direction. It is interesting to note that shock-wave and ultrasonic relaxation studies for $He–H_2$ also predict about 10^4—10^5 for the ratio of vibrational[9] to the rotational[10] relaxation times.

In the final step of Figure 1 the differential cross-sections can be introduced into equations (5) and (6) to compute rate constants, which can be compared directly with certain experiments or can be combined with the hydrodynamic equations to predict the outcome of a more complicated flow experiment (*e.g.* nozzle expansion). Incidentally, Figure 1 also applies in an analogous way to the problem of determining rate constants for chemical reactions.

The arrows in the flow diagram of Figure 1 indicate the natural 'direction' in which the calculations can be performed. In general, each step is extremely difficult to reverse or invert mathematically. For example, in the case of the first step this would mean that one would attempt to determine the coulomb law by 'inverting' potential-energy curves. However, as indicated in the diagram, one step can now be 'inverted' under certain favourable conditions. This is the step leading from the potential to the cross-section in the case of purely elastic

[7] H. Fremerey and J. P. Toennies, to be published.
[8] M. D. Gordon and D. Secrest, *J. Chem. Phys.*, 1970, **52**, 120.
[9] P. F. Bird and W. D. Breshears, *Chem. Phys. Letters*, 1972, **13**, 529.
[10] R. M. Jonkman, G. J. Prangsma, I. Ertas, H. F. P. Knaap, and J. J. M. Beenaker, *Physica*, 1968, **38**, 441.

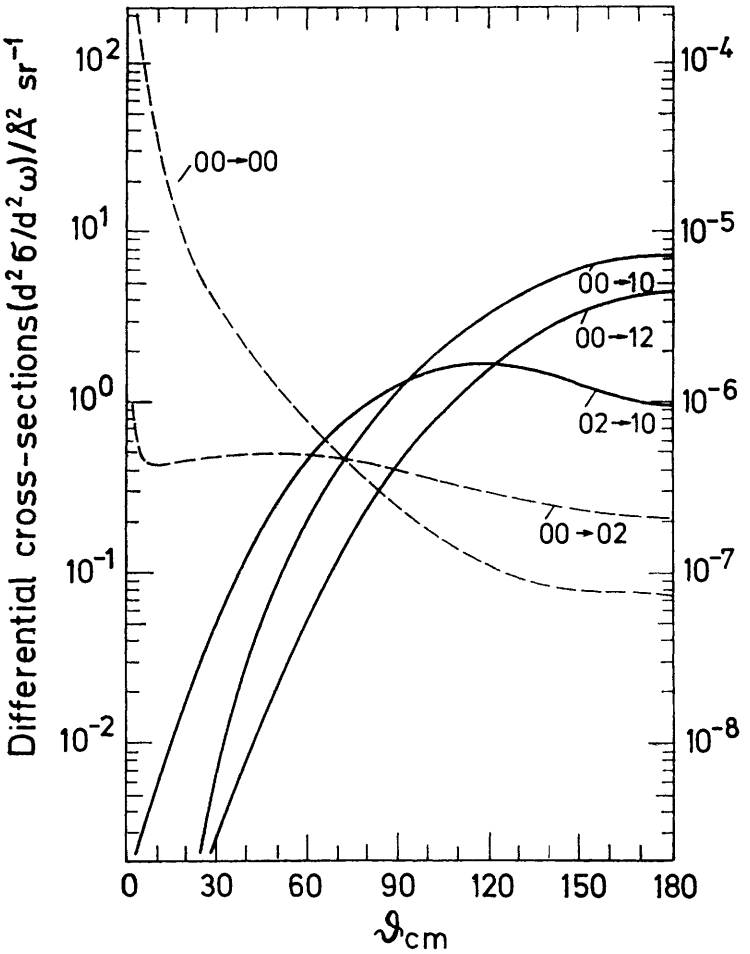

Figure 2 *The calculated differential elastic and inelastic cross-sections* $(n_1, j_1 \rightarrow n_t, j_t)$ *for the scattering of* He *from p-*H_2 *at* $E_{cm} = 1.09$ eV *are shown as a function of the scattering angle.*[7] *The elastic and rotationally inelastic cross-sections are plotted to the scale at the left whereas the vibrationally inelastic cross-sections are plotted to the scale at the right*

scattering.[11] Thus it is now possible to determine the spherically symmetric potential between two atoms, of which one is in a ^1S state, without recourse to one of the well-known potential models (*e.g.* Lennard-Jones).[12]

The disadvantage of the theoretical method stems from the fact that, because of the long computer times required, the first step – the calculation of potential

[11] U. Buck, *Rev. Mod. Phys.*, 1974, **46**, 369.
[12] J. P. Toennies, *Faraday Discuss. Chem. Soc.*, 1973, No. 55, p. 129.

hypersurfaces – cannot at present be accurately performed for systems with more than four electrons. Also, for the same reason, both partners should have closed shells. Only two systems fall into this category: $He–H_2$ and $Li^+–H_2$. The systems $H^+–H_2$ and $H–H_2$, although they have fewer electrons, suffer from the fact that open shells are encountered.

In view of this situation, one of the major goals of experimental studies is to explore the potential hypersurface. Once the hypersurface can be 'measured' then all the desired bulk properties can be obtained as indicated in Figure 1. Obviously, one of the most direct ways to explore the hypersurface is provided by beam-scattering experiments, in which a wealth of information in the form of the energy and angular dependence of the differential scattering cross-sections for all desired transitions can be obtained. Then by 'trial and error' or some other more direct procedure a hypersurface consistent with the experiments can be ascertained.

Inelastic cross-sections can be used to characterize certain parts of the potential hypersurface. This can be seen rather simply by considering Figure 3, in which the scattering angles and collision co-ordinates of a typical collision trajectory are shown. If we assume for simplicity that the molecule does not vibrate during a collision, then we see that during a collision a range of R and γ values are probed. The deflection observed in the elastic cross-section depends mostly on the R-dependence of $V(R, r, \gamma)$. In order for rotational excitation to take place, a torque whose magnitude depends on the 'strength' of the γ-dependent part of the potential must be applied to the molecule. In similar fashion, a force along the r direction is required to produce vibrational excitation.

C. Inelastic Scattering Experiments.—Figure 4 shows a simple schematic diagram of a crossed-beam scattering experiment. The entire apparatus is in a vacuum ($\sim 10^{-6}$ Torr) such that the mean free path is much greater than the dimensions of the apparatus. Thus the molecules in the two beams do not undergo collisions except in the scattering region, and once scattered are not deflected by subsequent collisions before reaching the detector. A detector sensitive to the molecules of interest is rotated about the scattering region and the measured intensity as a function of scattering angle is directly proportional to the differential scattering cross-section in the laboratory system. In general, the detection of chemical reaction products is comparatively easy since such products have a different mass from the reactants and can be separated with the aid of a mass spectrometer. The unique detection of inelastic events is, however, considerably more difficult. Thus relatively few studies have been reported. Most of the published work on inelastic scattering is surveyed in Table 1 (p. 416).[13–36]

[13] J. P. Toennies, 'Molecular Beam Scattering Experiments on Elastic, Inelastic and Reactive Collisions', in Vol. VIA of 'Physical Chemistry, an Advanced Treatise', Academic Press, New York, 1974.
[14] (*a*) J. P. Toennies, *Discuss. Faraday Soc.*, 1962, No. 33, p. 96; (*b*) *Z. Physik*, 1965, **182**, 257; (*c*) *ibid.*, 1966, **193**, 76.
[15] A. R. Blythe, A. E. Grosser, and R. B. Bernstein, *J. Chem. Phys.*, 1964, **41**, 1917.
[16] (*a*) P. B. Scott and T. R. Mincer, *Entropie*, 1969, **30**, 170; (*b*) P. B. Scott, T. R. Mincer, and E. P. Muntz, *Chem. Phys. Letters*, 1973, **22**, 71.
[17] D. Beck and H. Foerster, *Z. Physik.*, 1970, **240**, 136.
[18] T. F. Moran, F. Petty, and G. S. Turner, *Chem. Phys. Letters*, 1971, **9**, 379.

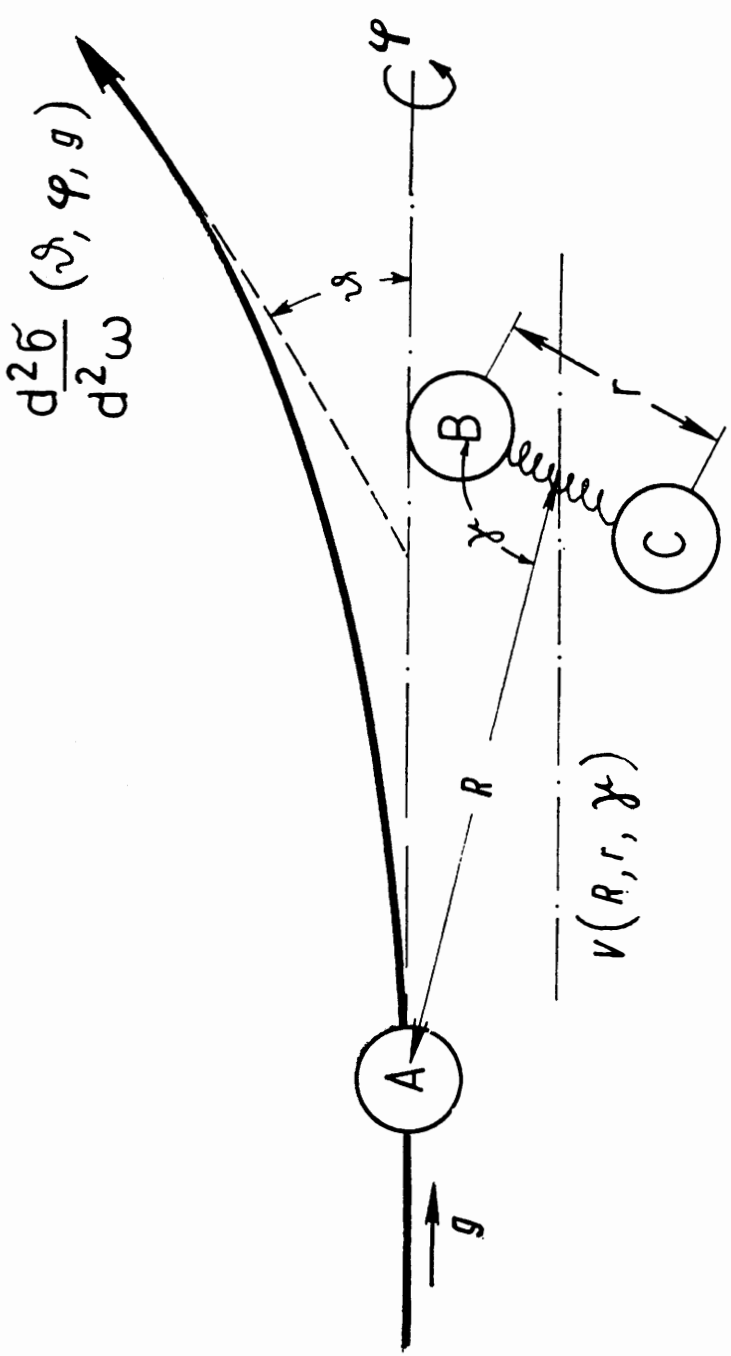

Figure 3 *Schematic diagram showing the potential and scattering co-ordinates for the scattering of an atom (or ion) from a diatomic molecule. During the collision trajectory (heavy solid line) the atom A probes the potential over a range of values of R, γ, and r*

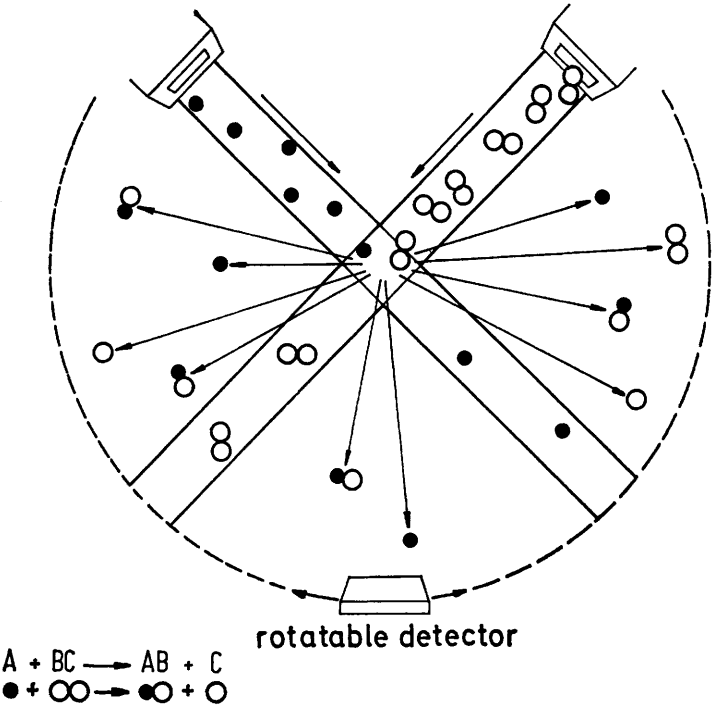

Figure 4 *Schematic diagram of a molecular- or ion-beam scattering experiment. The entire apparatus is in a vacuum with a pressure better than* 10^{-6} Torr. *The measurement of the laboratory differential cross-section for elastic, inelastic, or reactive scattering requires that the detector be sensitive only to those particles which have undergone the scattering process of interest*

[19] H. E. van den Bergh, M. Faubel, and J. P. Toennies, *Faraday Discuss. Chem. Soc.*, 1973, No. 55, p. 203.
[20] A. M. G. Ding and J. C. Polanyi, *Faraday Discuss. Chem. Soc.*, 1973, No. 55, p. 225.
[21] R. Böttner, U. Ross, and J. P. Toennies, *Faraday Discuss. Chem. Soc.*, 1973, No. 55, p. 221.
[22] J. M. Farrar, J. M. Parson, and Y. T. Lee, Proceedings IV International Symposium on Molecular Beams, Cannes, 1974.
[23] H. Udseth, C. F. Giese, and W. R. Gentry, *J. Chem. Phys.*, 1974, **60**, 305.
[24] P. F. Dittner and S. Datz, *J. Chem. Phys.*, 1968, **49**, 1969; 1971, **54**, 4228.
[25] H. van Dop, A. J. H. Boerboom, and J. Los, *Physica*, 1971, **54**, 223.
[25a] W. L. Dimpfl and B. H. Mahan, *J. Chem. Phys.*, 1974, **60**, 3238.
[26] T. F. Moran and P. C. Cosby, *J. Chem. Phys.*, 1969, **51**, 5724.
[27] P. C. Cosby and T. F. Moran, *J. Chem. Phys.*, 1970, **52**, 6157.
[28] F. Petty and T. F. Moran, *Chem. Phys. Letters*, 1970, **5**, 64.
[29] M. H. Cheng, M. H. Chiang, E. A. Gislason, B. H. Mahan, C. W. Tsao, and A. S. Werner, *J. Chem. Phys.*, 1970, **52**, 6150.
[30] F. Petty and T. F. Moran, *Phys. Rev.*, 1972, **A5**, 266.
[31] H. J. Loesch and D. R. Herschbach, *J. Chem. Phys.*, 1972, **57**, 2038.
[32] R. David, M. Faubel, and J. P. Toennies, *Chem. Phys. Letters*, 1973, **18**, 87.
[33] H. Udseth, C. F. Giese, and W. R. Gentry, *Phys. Rev.*, 1973, **A8**, 2483.
[34] (*a*) T. Donohue, M. S. Chou, and G. A. Fisk, *Chem. Phys.*, 1973, **2**, 271; (*b*) *ibid.*, *J. Chem. Phys.*, 1972, **57**, 2211; (*c*) F. F. Crim, M. S. Chou, and G. A. Fisk, *Chem. Phys.*, 1973, **2**, 283.
[35] R. Böttner, Max-Planck-Institut für Strömungsforschung, Göttingen, Bericht 105/1974, Germany.
[36] R. P. Mariella, D. R. Herschbach, and W. H. Klemperer, to be published.

Table 1 *Survey of low-energy inelastic scattering experiments*

(A) *Rotational Excitation (in chronological order)*

	Collision Processes[a]	E_{cm}/eV	*c.m. Scattering Angle*	$\frac{d^2\sigma}{d^2\omega}$/Å^2 sr^{-1} [b]	*Method*[c]	*Ref.*
R	$TlF(j_i) + X \rightarrow TlF(j_f) + X$; $j_i, j_f = 1, 2$, or 3 X = rare gas, CH_4, SF_6, H_2, O_2, N_2, N_2O, or H_2O	0.02	0—4°	10^2—10^4	SS: electrostatic quadrupole	14
R	$D_2(j = 2) + K \rightarrow D_2(j_f = 0) + K$	0.02	108°	$\sim 10^{-2}$	EC: velocity selectors	15
(R)	$N_2(j_i) + Ar \rightarrow N_2(j_f) + Ar$	10^{-2}	9—21°	—	SS: electron beam fluorescence spectroscopy	16
	$CO_2 + K \rightarrow CO_2 + K$	0.1	6—28°	0.3—4 ($\sigma_{inel} \simeq 2$—14 Å^2)	EC: velocity selectors	17
R	$CO^+(j_i \simeq 9) + Ar \rightarrow CO^+(j_f \simeq 30) + Ar$	3, 2, and 8	0—34°	—	EC: energy analysers	18
R	$H_2(j_i = 0, 1) + Li^+ \rightarrow H_2(j_f = j_i + 2) + Li^+$	0.6	14°, 23°, 32°	—	EC: TOF	19
(R)	$HCl(j_i, n_i) + Ar \rightarrow HCl(j_f, n_f) + Ar$ $j_i = 0$—15, $n = 0$ or 1	1.3	undefined	—	SS: i.r. spectroscopy	20
	$N_2(j_i \simeq 1)$ [CO] $+ Li^+ \rightarrow N_2(j_f) + Li^+$	4—8	35—55°	$\sum_{j_f} \frac{d^2\sigma}{d^2\omega} \simeq 0.6$ ($E_{cm} = 5.2$eV, $\vartheta = 37°$)	EC: TOF	21
	$CO_2[N_2O] + Ar \rightarrow CO_2 + Ar$	0.08	0—180°	—	EC: TOF	22
	$AB + H^+ \rightarrow AB + H^+$ AB = HF, HCl, N_2, or CO	10—30	4—30°	—	EC: energy analysis	23

[a] An R prior to the entry denotes that the quantum transition has been resolved. (R) implies that although quantum resolution is available, the transitions can nevertheless not be identified.

[b] If there is no entry, only relative differential cross-sections have been measured.

[c] SS denotes state-selection method and EC denotes energy-change method.

(B)	*Vibrational Excitation (in chronological order)*					
	$H_2, D_2 + M^\circ(M^+) \rightarrow H_2, D_2 + M^\circ(M^+)$ M = Li, Na, or K	3—35 5—60 0.7—17	180°	($\sigma_{inel} \simeq 10$ Å^2)	EC: TOF	24 25 25[a]
R	$D_2(n_i = 0) + Ar^+ \rightarrow D_2(n_f = 1 \text{ or } 2) + Ar^+$	11—17	0°	($\sigma_{inel} \approx 0.5$ Å^2)	EC: energy analysis	26
R	$O_2(n_i = 0) + O^+ \rightarrow O_2(n_f = 1, 2, \text{or } 3) + O^+$	8.8	0—38°	($\sigma_{inel} \approx 28$ Å^2)	EC: energy analysis	27
R	O_2^+ (undefined) + Ar → O_2^+ ($\Delta n = 1, 2, etc.$) + Ar	7.5	0—45°	—	EC: energy analysis	27
	$H_3^+ + Ne \rightarrow H_3^+ + Ne$	14	0—11.5°	—	EC: energy analysis	28
	$NO^+[O_2^+] + He \rightarrow NO[O_2^+] + He$	4—25	30—180°	—	EC: energy analysis	29
R	$CO^+(n \simeq 0) + Ar \rightarrow CO^+$ ($n_f = 1 \ldots 10$) + Ar	1—15	0—42°	—	EC: energy analysis	30
	$CsI + Ar \rightarrow CsI + Ar$	0.28—0.9	80—170°	($\sigma_{inel} \simeq 10$ Å^2)	EC: TOF	31
R	$H_2(n = 0) + Li^+ \rightarrow H_2(n = 1, 2, \text{or } 3) + Li^+$	3.7—8.8	215—170°	0.13($E_{cm} = 3.65$ eV, $\vartheta = 180°$)	EC: TOF	32
R	$H_2(n = 0) + H^+ \rightarrow H_2(n = 1, 2, \text{or } 3) + H^+$	4—21	6—22°	—	EC: energy analysis	33
	KBr + A(Mol) → KBr + A(Mol) A = Ne or Ar; Mol = N_2, CO, CO_2, H_2O, NH_3, or MeOH	0.05	50—80°	($30 \lesssim \sigma_{inel} \lesssim 300$ Å)	EC: velocity selector	34
R	$N_2[CO](n_i = 0) + Li^+ \rightarrow N_2[CO](n_f = 1 \text{ or } 2) + Li^+$	4—8	35—55°	—	EC: TOF	35
(R)	LiF(1100 K) + Mol → LiF($j_f = 1$, $n_f = 0, 1, 2, 3$) + Mol Mol = H_2O, SF_6, NH_3, or $CHFCl_2$	0.1	25, 45°	$\gtrsim 0.02$	SS: r.f. Rabi spectroscopy	36

Table 1 is divided into two parts. In the first part, studies of rotational excitation and in the second part studies of vibrational excitation are listed. The first column indicates the scattering partners. The letter R before the scattering process indicates that a specified quantum transition was resolved. The next columns list the collision energies and scattering angles explored. Where available, cross-section data are listed in the fourth column, and finally the method employed is given in the fifth column.

Essentially two fundamentally different experimental techniques are used.[13] The one is the 'State Selecting' (SS) method and the other the 'Energy Change' (EC) method. In the ideal state-selecting experiment the molecules are prepared in a definite state before scattering and the scattered molecules are analysed for their final rotational and/or vibrational state by an appropriate 'state filter', which permits only molecules in the desired state to arrive at the detector. State-selection experiments use focusing properties of electric fields, optical fluorescence, i.r. spectroscopy, and electron beam fluorescence. The resolving power of these experiments is generally very high. However, they are usually only applicable to special molecules, and the detection efficiency is very low. In some cases where spectroscopic techniques are used the molecules were not prepared in a specified initial state. [These experiments are indicated by an (R) in Table 1.] Here the interpretation of the experiments in terms of cross-sections is usually not unique.

In the energy-change experiments, the final velocity of one of the particles after the collision is measured. The initial velocities of both particles being sufficiently well defined, the inelastic energy loss observed after the collision can be used to determine which vibrational or rotational state has been excited. The big advantage of this method is its universality. On the other hand, the experiments are difficult to perform and, consequently, the state-resolving power is usually poor compared with that of the state-analysing methods. This is the reason why in Table 1, of the 11 experiments with an R-rating, only one ($K + D_2$) is a neutral scattering experiment based on the EC method. In this experiment only a very weak inelastic peak was, barely, resolved.

Whereas the neutral particle 'energy loss' experimental techniques are still in an early stage, Table 1 shows that a large number of analogous experiments with ions have been carried out. The chief advantages of ions over neutrals are that, once produced, they are easily accelerated to energies of several eV. Energies in this range are often hard to achieve with neutral particles, and as suggested by Figure 2 are probably needed in many cases to have a high probability of vibrational excitation. The other big advantage is that they can be detected with near 100% efficiency with an open electron multiplier. Since the theoretical treatment for low-energy ion–molecule scattering is essentially the same as for neutrals, ion–molecule experiments are well suited for prototype studies of inelastic collision processes with translational- to internal-energy transfer.

For detecting the energy loss in ion-scattering experiments, both energy analysis by electric (and sometimes magnetic) fields and the time-of-flight (TOF) method have been used. Since the ions can be produced from almost any atom or molecule, a large variety of collision partners can be studied.

Being the simplest of all molecules, scattering from H_2 is of greatest interest. Furthermore, H_2 has the experimental advantage of the widest rotational and vibrational energy-level spacing of all molecules*. The simplest and therefore theoretically most attractive ionic collision partners for the H_2 molecule are the H^+, D^+, and Li^+ ions. The four-electron Li^+–H_2 potential hypersurface[38,39] and to a lesser extent the two-electron H^+–H_2 hypersurface are known from quantum chemical calculations.[40] In the latter system, the H^+–H_2 and H–H_2^+ potential surfaces lie close together, and 'cross' one another when the H_2 intramolecular distance is somewhat extended. This additional inelastic process, which is especially difficult to treat theoretically, has to be accounted for in order to compare scattering experiments on H^+–H_2 with theory. This problem does not arise for Li^+–H_2, where up to collision energies of 10 eV only pure rotational and vibrational excitation is energetically possible (dissociation can also occur above 4.5 eV). For this reason we will discuss the inelastic scattering in Li^+–H_2 in more detail in the next section. These experiments provide a direct test of the theoretical assumptions involved in going from the upper left-hand corner of Figure 1 to the differential cross-sections.

2 Experimental Inelastic Scattering Studies of Li^+–H_2

A. Apparatus.—In our experiments we have chosen to use the time-of-flight (TOF) energy-loss technique.[41] The time-of-flight method offers the advantages of a large resolving power at low velocities, and the possibility of measuring the energy loss absolutely by measuring the flight times for two different flight paths, the differences of which can be precisely determined. The apparatus is shown in Figure 5. The ^7Li ions are produced by an isotopically pure surface-ionization source. The ions are then accelerated toward the entrance slit of a 127° electrostatic cylindrical energy analyser with a mean radius of 5 cm and an energy resolution of $\Delta E/E = 0.4\%$ (fwhm). The chopping of the beam is performed by applying a d.c. voltage to the condenser plates, large enough to deflect the beam away from the slit. This voltage is then switched off for a short time to allow the ions to pass into the scattering centre. The length of the ion bursts produced in this way is typically 50 ns at a Li^+ energy of 15 eV.

In order to resolve specified quantum transitions the target beam must fulfil two requirements: (1) the target molecules should all be in one quantum state, and (2) the target-beam velocity spread and angular spread should be as narrow as possible. Both requirements can only be fulfilled by using a skimmered nozzle beam, which is also shown in Figure 5. The cooling in the expansion

* For example, the $j = 0 \rightarrow j = 2$ and $j = 1 \rightarrow j = 3$ rotational energy-level spacings are 0.045 eV and 0.075 eV, respectively; the $n=0 \rightarrow n = 1$ vibrational level spacing is 0.51 eV.[37]

[37] W. Kolos and L. Wolniewicz, *J. Chem. Phys.*, 1968, **49**, 404.

[38] (*a*) W. A. Lester, *J. Chem. Phys.*, 1970, **53**, 1511; (*b*) *ibid.*, 1971, **54**, 3191; (*c*) *ibid.*, 1972, **57**, 3028.

[39] W. Kutzelnigg, V. Staemmler, and C. Hoheisel, *Chem. Phys.*, 1973, **1**, 27.

[40] I. G. Csizmadia, R. E. Kari, J. C. Polanyi, A. C. Roach, and M. A. Robb, *J. Chem. Phys.*, 1970, **52**, 6205.

[41] J. Schöttler and J. P. Toennies, *Z. Physik.*, 1968, **214**, 472.

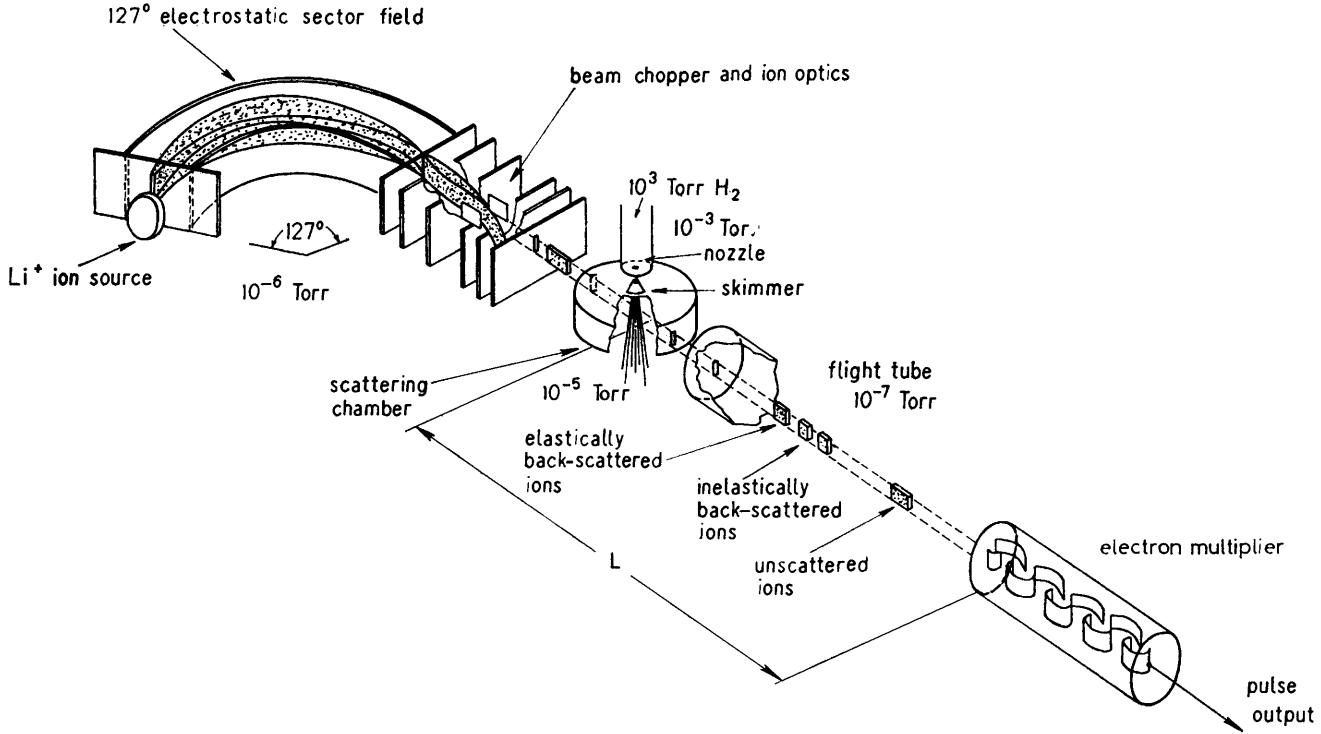

Figure 5 *Schematic diagram of the time-of-flight apparatus used for studying inelastic scattering in* Li^+–H_2. *The* Li^+ *beam source is at the left. The ion beam energy is selected by a* 127° *electrostatic sector field. The ion beam is then electrically chopped and passed into the scattering chamber, where it is crossed with an* H_2 *nozzle beam. The flight path length L is variable between* 50 *and* 170 cm

reduces the rotational temperature sufficiently that most of the molecules are in the ground rotational state.[42] An angular collimation of 3—4° fwhm is achieved by the skimmer, which removes all beam molecules with greater divergence. In this way the primary beam ions 'see' a narrow (2 mm) target (pressure $\simeq 10^{-2}$—10^{-3} Torr) with a translational temperature (along the incident beam direction) of only 3 K. After scattering, the ions are detected in a plane perpendicular to the target beam.[43] They enter a free-flight region and are detected by an open secondary electron multiplier. The absolute flight time of each individual ion is measured (in steps of 10^{-7} s) by a crystal clock circuit and stored in a mini-computer (DEC, PDP-8/L) in the form of a time-of-flight histogram. Since the total flight time is usually considerably greater than 10^{-5} s, a resolving power of better than 1% is achieved.*

B. Preliminary Measurements.—As a first step in probing the interaction potential, the angular distribution of scattered ions was measured by rotating the detector about the secondary beam and counting all ions without analysing for their times of flight. The quantity measured in this way is the total laboratory differential cross-section defined by:

$$\frac{\mathrm{d}^2\sigma^{j=0}}{\mathrm{d}^2\Omega_{\mathrm{tot}}}(\theta) = \sum_{j_t} \frac{\mathrm{d}^2\sigma^{j_i=0\to j_t}}{\mathrm{d}^2\Omega}(\theta) \qquad (7)$$

Since a cold (T = 77 K) para-hydrogen target was used in the experiment the sum in equation (7) extends from $j = 0$ (the initial state) over all even final rotational states which contribute appreciably to the sum. Figure 6 compares the results of such a measurement at a centre-of-mass energy of 0.6 eV[44] with the quantum-mechanical cross-sections[45] based on an accurate *a priori* calculated hypersurface.[38b] The quantum-mechanical cross-sections were transformed into the laboratory system for direct comparison.

The large maximum at $\theta = 6°$ corresponds to the primary rainbow, which in the centre-of-mass system occurs at about $\vartheta_{\mathrm{cm}} = 27°$. This phenomenon has a simple classical interpretation, which enables one to attribute all scattering events at this and smaller angles to an interaction with the long-range attractive part of the potential only.[12,46] The scattering to the right of the rainbow can be attributed to deflections produced largely by the repulsive part of the potential. In the approximation of classical scattering theory and considering only elastic scattering, one can assign to each scattering angle a distance of closest approach R_{min} at which most of the interaction and deflection takes place.

* Other factors affecting the resolving power are the length of the scattering region ($\Delta L/L = \frac{2\text{ mm}}{500\text{ mm}} = 0.4\%$) and the solid angle of the detector ($\Delta^2\Omega = 2 \times 10^{-5}$ sr).

[42] R. J. Gallagher, Ph.D. Thesis Yale University, 1972.
[43] E. F. Greene, M. H. Lau, and J. Ross, *J. Chem. Phys.*, 1969, **50**, 3122.
[44] M. Faubel and Kl. Rudolph, unpublished observations.
[45] W. A. Lester and J. Schaefer, personal communication.
[46] H. Pauly and J. P. Toennies, *Adv. Atom. Mol. Phys.*, 1965, **1**, 195.

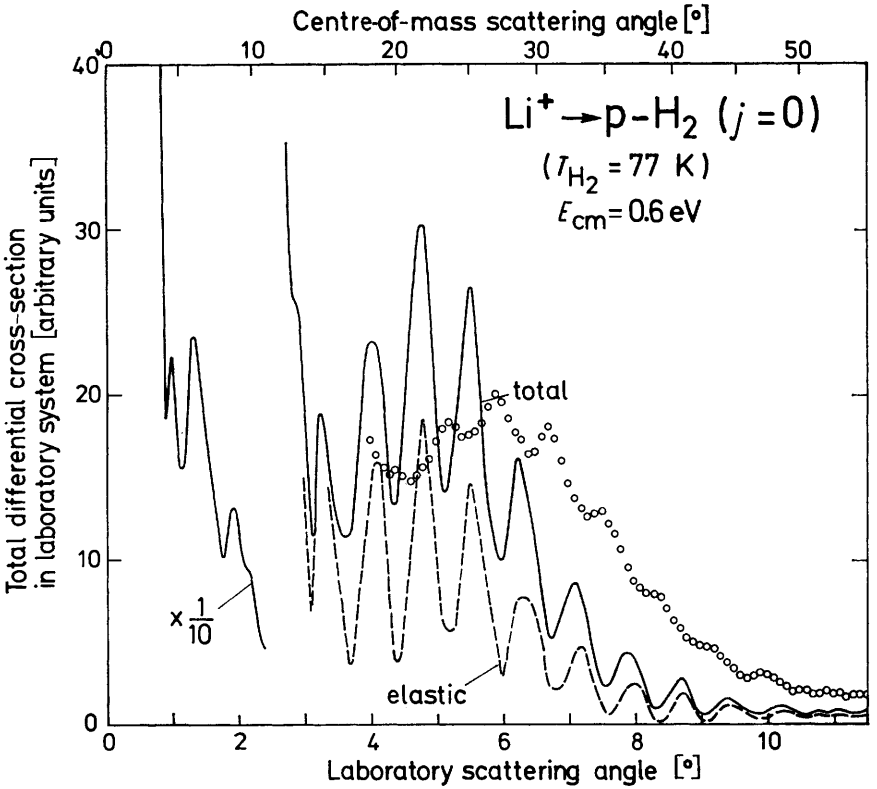

Figure 6 *The quantum-mechanically calculated total differential cross-section (solid line) is compared with the measured cross-section (points with connecting curve) at* E_{CM} = *0.6 eV. The calculated cross-sections were converted to the laboratory system by an approximate procedure which did not take account of apparatus smearing and the target motion. The dashed line shows the elastic* ($j = 0 \rightarrow 0$) *contribution to the theoretical total cross-section*

With increasing angle, R_{min} becomes smaller, until at the largest angle $\vartheta_{cm} = 180°$, R_{min} is given by $V(R_{min}) = E_{cm}$ (central collision). Thus to a good approximation scattering events at each angle provide information about the nature of the potential in a definite region of R. The undulations in the theoretical cross-section are due to quantum interferences. The amplitudes in the measured curve are considerably reduced by apparatus smearing. Nevertheless, they are sufficiently well resolved to show excellent agreement with the theoretical curve provided the experimental curve is shifted by about 1.1° to smaller angles. This shift suggests that the well depth of the *a priori* potential hypersurface is too small by about 16%.

The upper part of Figure 7 shows the result of a typical 16 hour TOF measure-

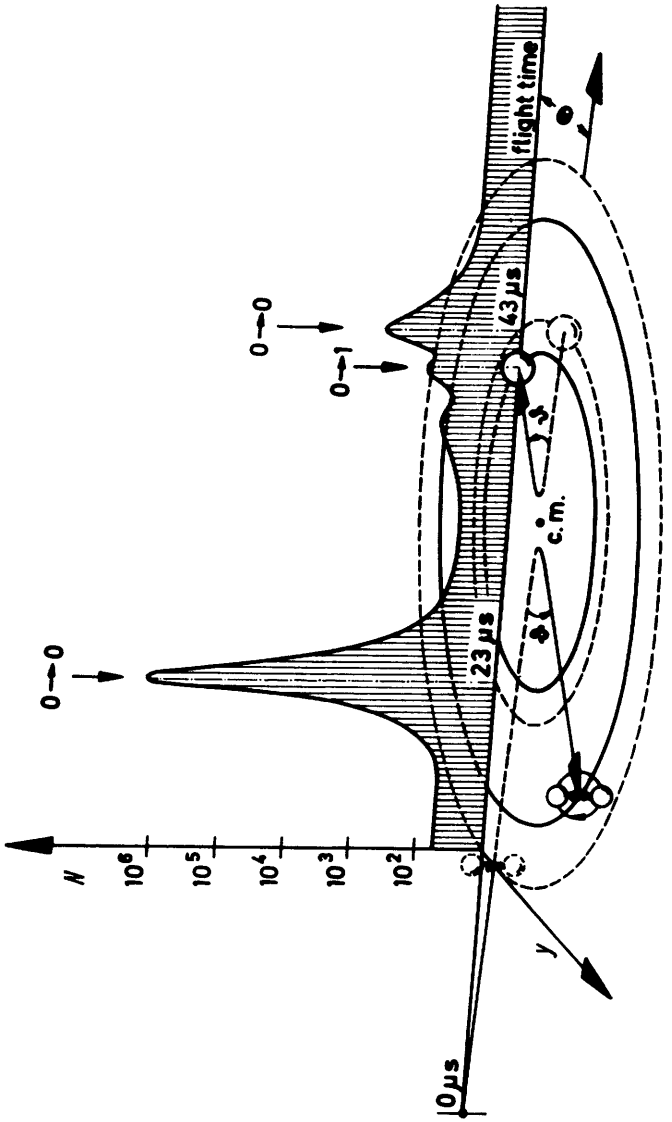

Figure 7 *Composite diagram showing a typical time-of-flight spectrum (at the top) and the identification of the individual peaks in terms of the corresponding scattering process in the centre-of-mass system (at the bottom). At the top the total number of ions counted in a* 100 ns *channel over a measuring time of* 16.5 h (E_{lab} = 16.3 eV, E_{cm} = 3.63 eV, $\theta = 3°$) *is plotted as a function of the total time of flight. The time dimension has been projected on to the two-dimensional laboratory space at the bottom to show the relative locations of the particles with respect to the centre of mass at a given instant. In the experiment only the* Li^+ *ion is observed*

ment for 16.3 eV $^7Li^+$ ions scattered at a laboratory angle of 3°.[32] The total number of ions counted in a 100 ns channel is plotted as a function of the time of flight. Since Li is heavier than the H_2, two peaks appear at one laboratory angle; the first, at the smaller time of flight (23 μs), corresponds to a c.m. forward-scattering angle $\vartheta_{cm} = 15°$ and the second peak at the larger time of flight (43 μs) corresponds to the c.m. backward-scattering angle, $\vartheta_{cm} = 167°$. While the forward peak does not show any remarkable structure, the backward peak exhibits two side peaks at the positions where vibrationally inelastic scattered ions are expected. The identification of the individual peaks in terms of the corresponding scattering process in the centre-of-mass system is shown schematically at the bottom of Figure 7. Here the time dimension has been projected on to the two-dimensional laboratory space to show the relative locations of the particles with respect to the centre of mass at a given instant in time.

Experiments of this type are difficult because of the very low scattering signals involved. In the typical experiment shown in Figure 7 about 2×10^9 ions entered the scattering region altogether. Because of the low scattering cross-section, scattering target density, and target depth, only about 1 in 10^3 ions are scattered. As is to be expected from Figure 2, most of these are scattered under small angles in the centre-of-mass system, and account for the large fast peak at 23 μs, with about 10^6 ions. Also in accord with Figure 2, the backward elastic peak is smaller by about 3 orders of magnitude. In the inelastic $n = 0 \rightarrow 1$ backward peak, which is relatively much larger than predicted for He–H_2 in Figure 2, a total of less than 10^3 particles is observed. This corresponds to a current of backward inelastic events of only 1 per minute.

C. Studies of Rotational Excitation.—To resolve the small energy losses associated with rotational quantum transitions, the following considerations lead to the choice of low energies and centre-of-mass scattering angles. At low energies E the apparatus resolution ΔE is greatest, since the relative energy resolution $\Delta E/E$ of the apparatus is constant. Small centre-of-mass angles have several advantages: firstly, apparatus smearing is least,[19] secondly, as indicated by Figures 2 and 7, the scattering cross-sections are expected to be largest at small angles. Lastly, as discussed in connection with Figure 6, results at angles less than the rainbow can be interpreted directly in terms of the long-range potential.

Figure 8 shows one of the first TOF spectra at 2.7 eV ($E_{cm} = 0.6$ eV), where nearly isolated rotational transitions were observed.[19] The half-width of the elastically scattered peak is equivalent to $20 \simeq 25$ meV energy resolution ($\Delta E/E \simeq 3\%$). Because of the intensity loss originating from the high resolution and very low primary beam energies, the inelastic signal amounted to only 1 ion in every 20 minutes. To compensate for this very low intensity, typical measuring times of 50—100 h were required for a single spectrum. The expected peak locations are indicated by arrows at the top of Figure 8. Normal hydrogen was used, so that transitions due to para- and ortho-hydrogen are observed. The spectrum shows a large elastic peak, attributed to both $j = 0 \rightarrow j = 0$ (25%) and $j = 1 \rightarrow j = 1$ (75%), and a smaller side peak, which can be attributed to

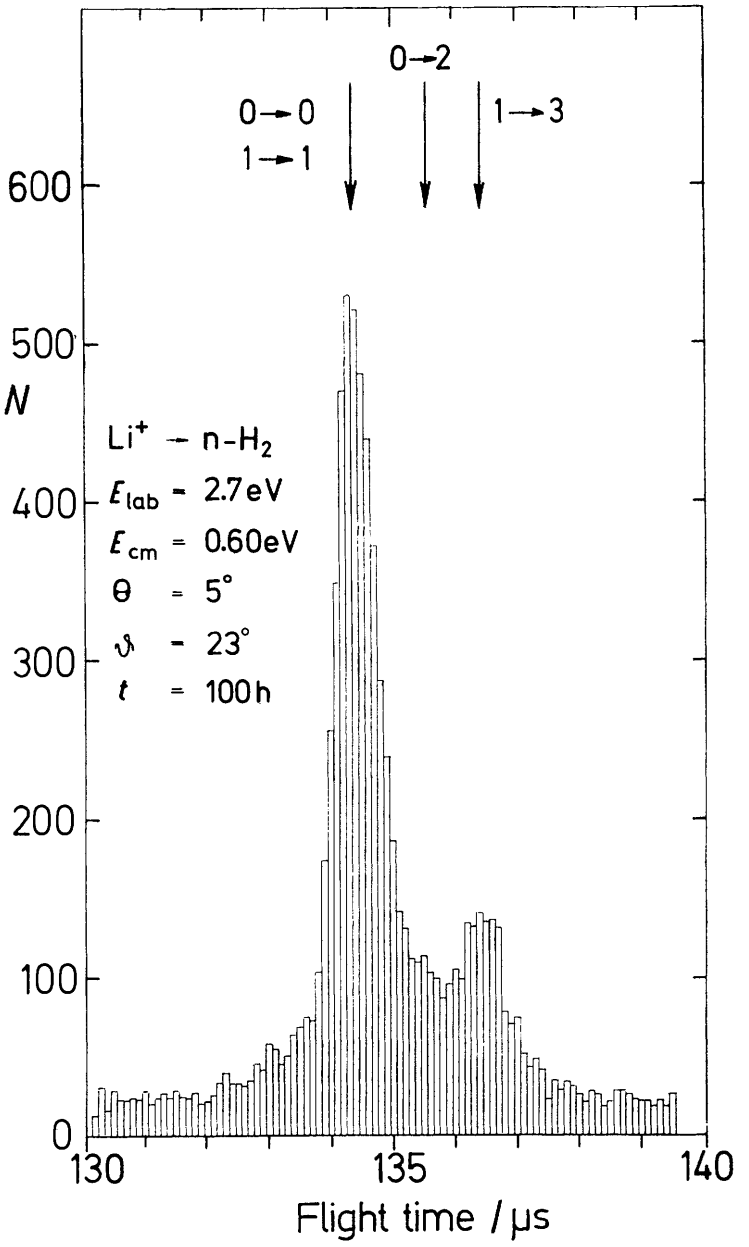

Figure 8 *Measured time-of-flight spectrum showing forward scattering at* $\theta = 5°$ ($\vartheta_{cm} = 23°$) *and* $E_{lab} = 2.7$ eV ($E_{cm} = 0.60$ eV).[19] *The arrows at the top show the calculated location of the elastic and inelastic maxima corresponding to the indicated rotational transitions* ($L = 115$ cm).

the $j = 1 \rightarrow j = 3$ transition. Since only 25% of the molecules are initially in $j = 0$, a peak at the position corresponding to $j = 0 \rightarrow 2$ is not observed. The cross-sections for higher rotational excitations with $\Delta j > 2$ have been observed to be at least five times smaller.[47]

The TOF spectrum contains very precise information on the inelastic cross-sections relative to the elastic cross-section. For comparison with theory it is most convenient to transform the experimental results into the centre-of-mass system. This transformation is performed by simulating the scattering process and the kinematical smearing occurring in the apparatus on a computer.[48] The following nine *known* apparatus distributions were included: incident beam energy and angular distributions (3 distributions), secondary beam velocity and angular distributions (3), start-time distribution produced by the beam chopper (1) and the detector geometry (2). The calculations were performed for various ratios of cross-sections in the centre of mass until a best fit of the data was obtained. Figure 9 shows that it was possible to fit closely the measured spectrum with such a simulated spectrum. The fit also shows that the 'filling' of the valley between the two observed peaks can be attributed to a 'buried' peak at the expected location of the $j = 0 \rightarrow j = 2$ transition.

Since the relative cross-sections are measured with the greatest accuracy, we have arbitrarily normalized the inelastic peaks to the elastic peak. Thus the following ratios are measured:

$$0 \rightarrow 2 \text{ peak, } \{[1/4(0 \rightarrow 2)]:[1/4(0 \rightarrow 0) + 3/4(1 \rightarrow 1)]\};$$
$$1 \rightarrow 3 \text{ peak, } \{[3/4(1 \rightarrow 3)]:[1/4(0 \rightarrow 0) + 3/4(1 \rightarrow 1)]\},$$

where $(0 \rightarrow 2)$ denotes $d^2\sigma^{0\rightarrow 2}/d^2\omega$ *etc.* Table 2 summarizes these measured ratios. Transition probabilities can be obtained from the measurements only by introducing the theoretical ratio $(1 \rightarrow 1)/(0 \rightarrow 0)$, which, surprisingly, is not equal to one. This was first shown by classical calculations[49] and has since been confirmed by quantum-mechanical calculations.[50,51d] These ratios and the transition probabilities P for $0 \rightarrow 2$ are greater than for $1 \rightarrow 3$, in agreement with the Massey criterion $\left[P \approx \exp\left(-\frac{\Delta E}{h}\tau\right), \text{ where } \tau \text{ is the collision time}\right]$.

D. Studies of Vibrational Excitation.—As suggested by Figure 2, vibrational excitation is usually expected to be most probable for large-angle – nearly backward – scattering in the centre-of-mass system. Also, in order to produce an observable amount of vibrational excitation, considerably greater relative

[47] H. E. van den Bergh and M. Faubel, unpublished observations.
[48] H. E. van den Bergh, M. Faubel, and J. P. Toennies, unpublished observations.
[49] G. D. Barg, G. M. Kendall, and J. P. Toennies, to be published.
[50] W. A. Lester and J. Schaefer, *J. Chem. Phys.*, 1974, **60**, 1672.
[51] (*a*) J. Schaefer and W. A. Lester, *Chem. Phys. Letters*, 1973, **20**, 575; (*b*) W. A. Lester and J. Schaefer, *J. Chem. Phys.*, 1973, **59**, 3676; (*c*) J. Schaefer, W. A. Lester, D. Kouri, and C. A. Wells, *Chem. Phys. Letters*, 1974, **24**, 185; (*d*) J. Schaefer and W. A. Lester, to be published.

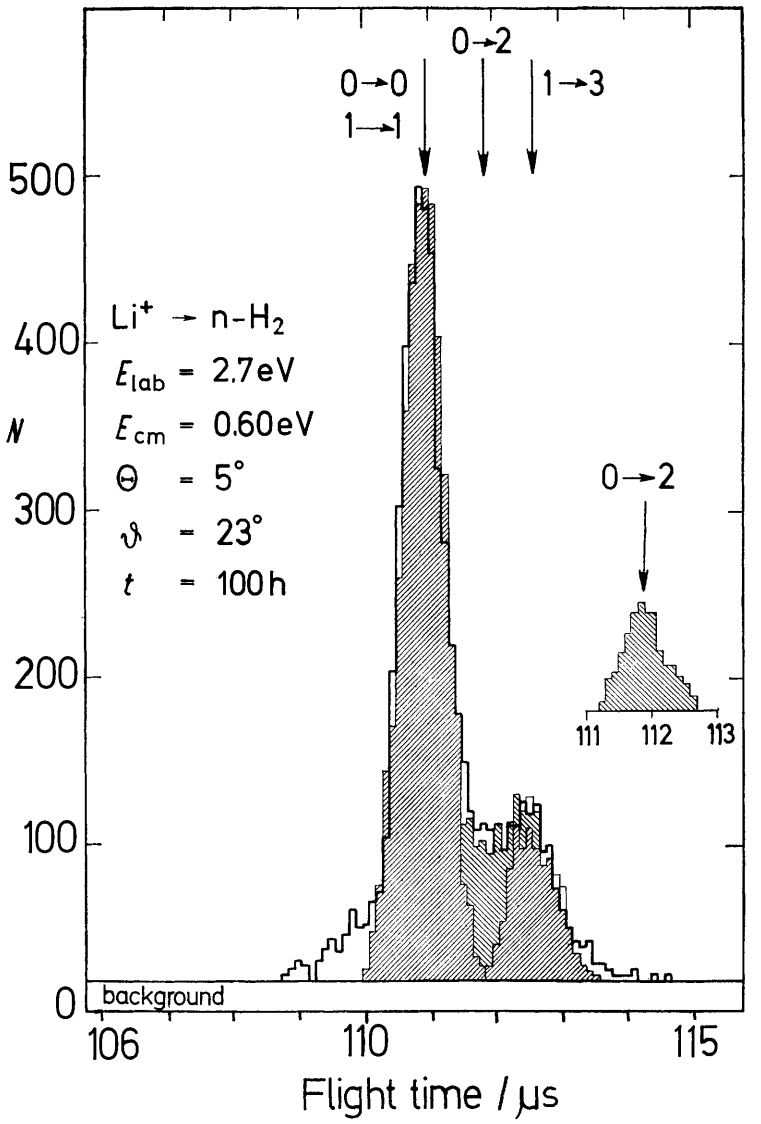

Figure 9 *Comparison of a best-fit computer-stimulated spectrum with a measured spectrum. All conditions, except L = 95 cm, are the same as in Figure 8. The three shaded regions are the calculated histograms for the elastic, j = 0 → 2, and j = 1 → 3 cross-sections. The insert shows the isolated j = 0 → 2 distribution*

Table 2 *Measured differential cross-section ratios R at* E_{cm} = 0.60 eV. *The errors are roughly* 30%. *The target is normal* H_2 *with ortho:para* = 3:1. *The ratios of the elastic cross-sections* (1 → 1) . (0 → 0) *are obtained from the best available theoretical calculations.*[50] *From these the transition probabilities P in the last column are obtained*[a]

Nominal Lab. Angle/°	*C.m. Angle and Uncertainty*	*Measured Ratios R*		*Theoretical Ratios of Elastic Cross-sections*	*Transition Probabilities P*	
		(0→2):{(0→0) + 3(1→1)}	3(1→3):{(0→2) + 3(1 + 1)}	(1 → 1):(0 → 0)	0 → 2	1 → 3
3	14 ± 1.5	0.068	0.068	1.518	0.274	0.076
5	23 ± 1.7	0.135	0.216	1.483	0.424	0.209
7	32 ± 1.9	0.132	0.184	1.773	0.451	0.180

[a] *e.g.* $P_{0\to 2} = \dfrac{R_{0\to 2}\left[1 + 3\dfrac{(1\to 1)}{(0\to 0)}\right]}{1 + R_{0\to 2}\left[1 + 3\dfrac{(1\to 1)}{(0\to 0)}\right]}$ where $R_{0\to 2}$ is the corresponding measured ratio of column 3.

energies will be required compared to those used in the studies of rotational excitation.

Evidence for vibrational excitation was already seen in Figure 7. In Figure 10

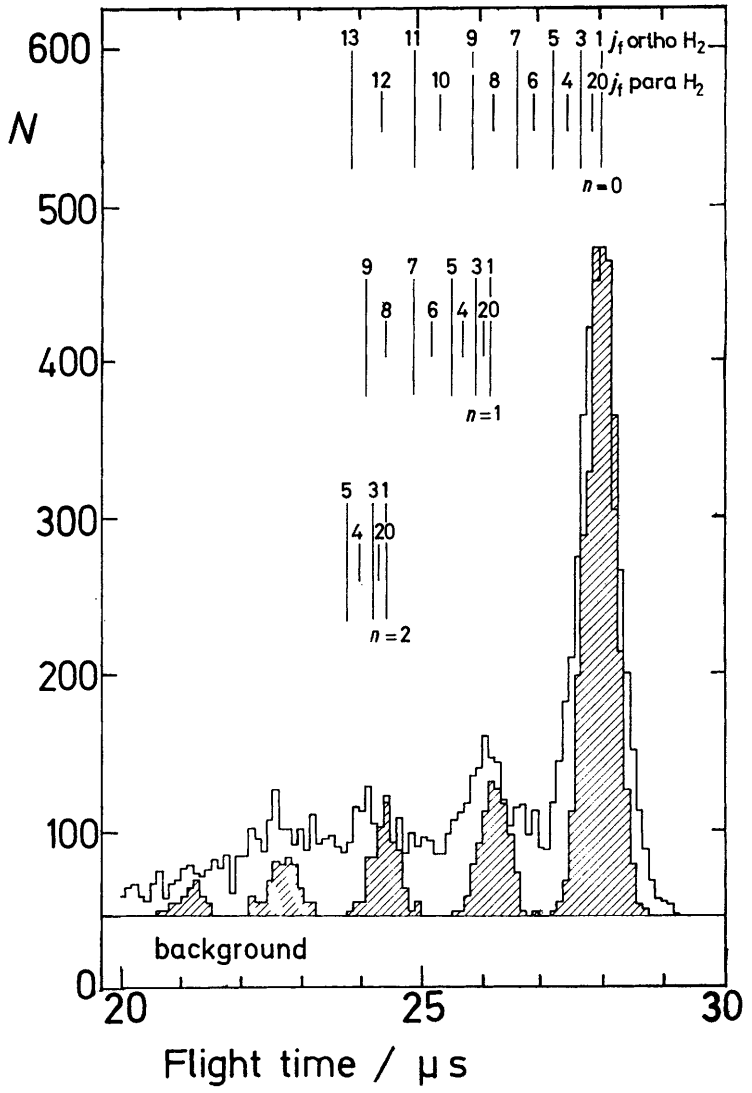

Figure 10 *Comparison of a best-fit computer-simulated spectrum with a measured spectrum for backward scattering* (E_{cm} = 3.6 eV, θ_{lab} = 3°, ϑ_{cm} = 167°, L = 73.9 cm, *measuring time* = 7 h). *The shaded spectra have been calculated assuming only vibrational excitation. The vertical lines at the top show the expected flight times for the various possible inelastic channels for the ortho and para components of the normal* H_2 *target. The experimental uncertainty in the absolute position of the flight time-scale corresponds to* ±0.3 μs

a better-resolved TOF spectrum (white histogram), showing only the backward portion of the spectrum, can be seen. Also shown at the top of Figure 10 are the expected locations of all possible inelastic maxima. The shaded histogram is a computer simulation of the backward spectrum obtained by assuming only vibrational excitation to occur in the experiment.[48] The good agreement between the observed secondary maxima and the calculated peak locations as well as the simulated spectra strongly suggest that these correspond to the vibrational transitions $0 \rightarrow 1$ and $0 \rightarrow 2$, *etc.* The resolving power is not sufficient to establish the exact amount of simultaneous rotational excitation accompanying these transitions. However, some qualitative information on these transitions can be obtained by carefully examining the spectra. Since the errors in the absolute measurement of the flight times are large enough to allow one to shift the measured curves by ± 300 ns, which corresponds roughly to the energy change for the $0 \rightarrow 2$ rotational transition, we cannot exclude these transitions in the primary and secondary backward peaks. However, the sharp drop off on the left-hand side of the peaks indicates that the probabilities of $\Delta j = 4$ and $\Delta j = 6$ transitions are smaller by at least a factor 5. That some rotational excitation is present can be seen from the difference between the computer-simulated and measured spectra, which is greatest on the left-hand side of the peaks. If there were no rotational excitation the agreement would be the same on both flanks of the peaks.

By allotting all of the intensity under each of the maxima to the corresponding vibrational transition, relative transition probabilities in the centre-of-mass system shown in Figure 11 were determined. Surprisingly, these results show only a small increase in the $n = 0 \rightarrow n = 1$ differential cross-section with increasing energy for angles greater than 150°. At smaller angles, however, the differences appear to be larger. Since the integral cross-section is given by $\sigma^{n=0\rightarrow 1} = 2\pi \int \mathrm{d}^2\sigma^{0\rightarrow 1}/\mathrm{d}^2\omega \sin\vartheta \mathrm{d}\vartheta$, the differences close to $\vartheta = 90°$ contribute most and can be expected to lead to a considerable increase in $\sigma^{0\rightarrow 1}$ with energy. This increase in cross-section with energy is in agreement with the Landau–Teller theory, which for essentially this reason predicts a $T^{-\frac{1}{3}}$ temperature dependence of the relaxation times, in good agreement with many bulk measurements.[1]

3 Comparison of *ab Initio* Theory and Experiment

A. Rotational Excitation.—The potential hypersurface for Li^+–H_2 has been calculated by Lester[38] and independently by Kutzelnigg, Staemmler, and Hoheisel.[39] Figure 12 shows the three-dimensional part – appropriate to rotational excitation – of this actually four-dimensional hypersurface. The potential is plotted as a function of the Li–H_2 distance R and the orientation angle γ. The intramolecular distance r of the two hydrogen atoms has been fixed at the hydrogen ground-state equilibrium position, and therefore the region of the hypersurface depicted is for the scattering of an atom from a rigid rotator. The mean well depth of the attractive part of the potential is about -150 meV.

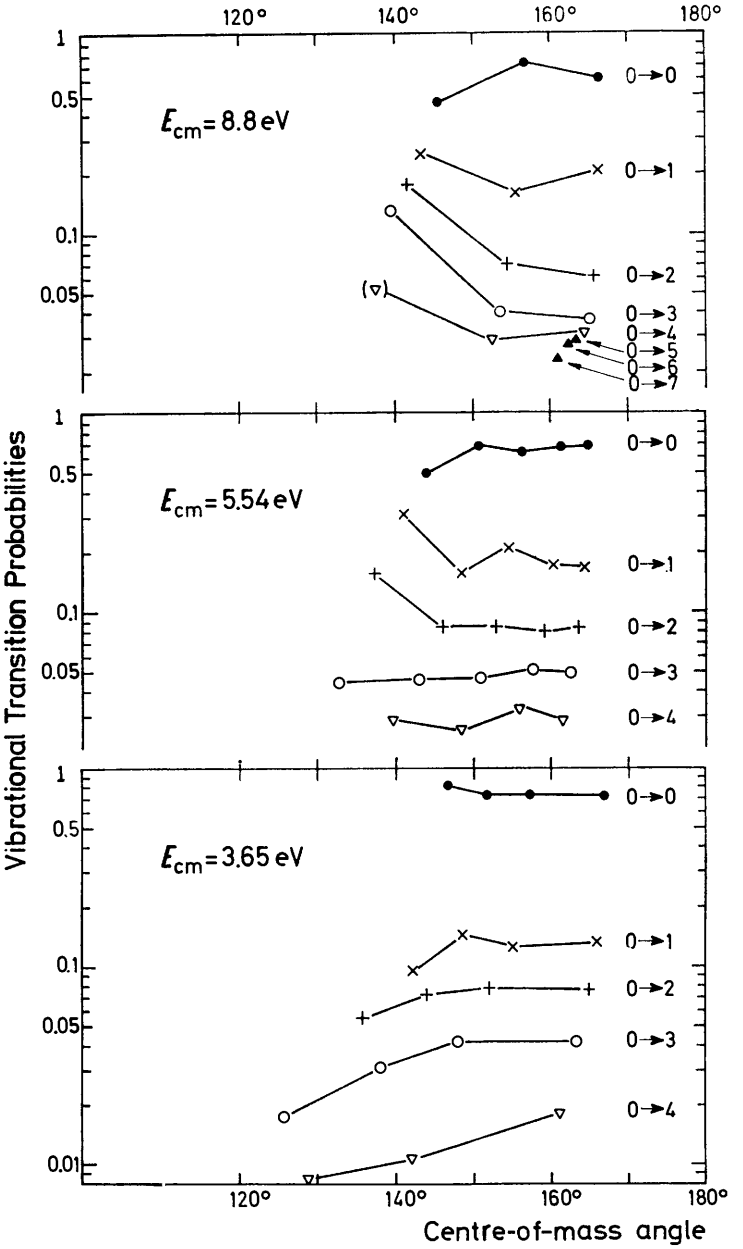

Figure 11 *Measured vibrational transition probabilities for three different c.m. energies are plotted as a function of the scattering angle. The transition probability is defined as the ratio of the differential cross-section for a given transition to the sum of differential cross-sections for all transitions*

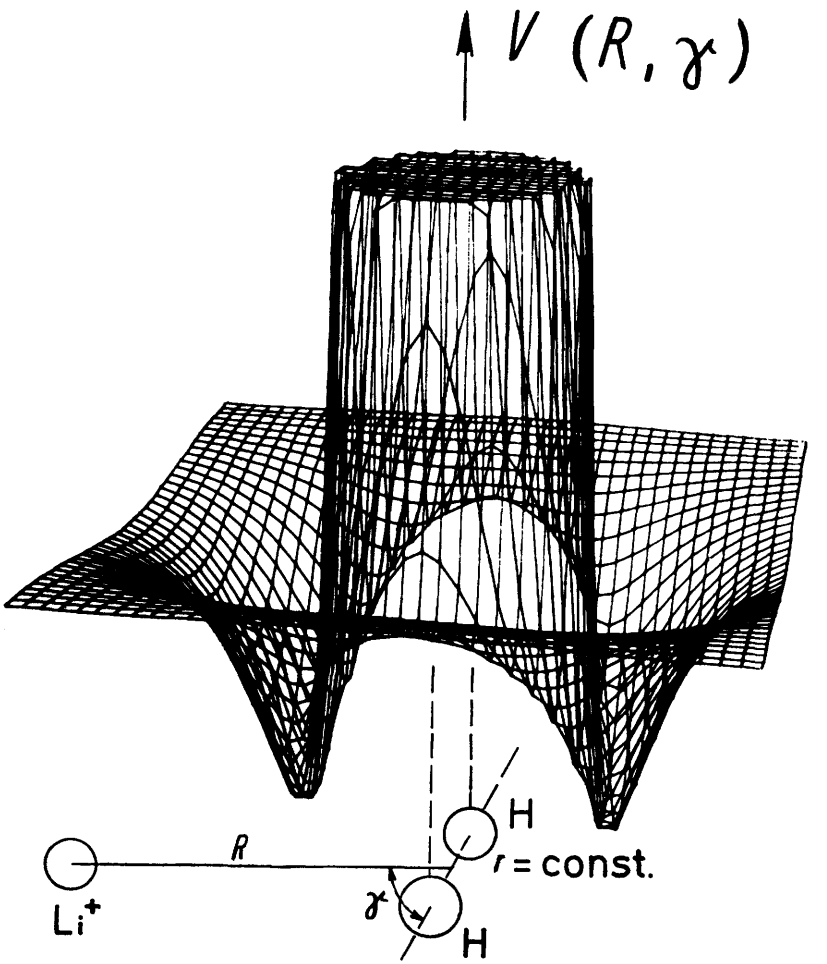

Figure 12 *The potential energy for a* Li^+ *ion approaching a rigid* H_2 *molecule* ($r = r_{eq}$) *is plotted as a function of the remaining potential co-ordinates R and* γ.[38a] *For* $\gamma = 90°$ *the potential well depth is* 250 meV, *but for* $\gamma = 0°$ *only* 50 meV

The depth changes from about −50 meV to −250 meV, depending on the orientation angle.

Close-coupling quantum-mechanical calculations of the differential inelastic cross-sections have been carried out on these hypersurfaces independently by two groups.[50–52] Furthermore, classical Monte Carlo trajectory calculations have also been done on the same surfaces and at the same energies.[49] The results

[52] P. McGuire, *Chem. Phys.*, 1974, **4**, 249.

of all three theoretical groups are in reasonable agreement. Typical calculated elastic and inelastic cross-sections based on quantum and classical mechanics are compared in Figure 13. In both approximations the elastic and inelastic $\Delta j = 2$ cross-sections show a definite rainbow.[53] Whereas the quantum calculations show a primary rainbow between 20 and 25° and a secondary rainbow at about 8°, the classical calculations show only one rainbow at about 40°. This shift in the classical rainbow angle is just the same as that observed in analogous comparisons of atom–atom elastic scattering cross-sections. The quantum-mechanical calculations exhibit the fast quantum-mechanical interference oscillations observed in the measurements of the total cross-section, discussed previously (Figure 6).

The classical calculations have moderately large statistical errors ($\lesssim 10\%$) and are averages over an angular region or 'bin' of width $\Delta\vartheta = 1°$.

In order to determine the cross-section ratios needed for comparison with experiment, the angular distributions for the $0 \rightarrow 0$, $1 \rightarrow 1$ as well as the $0 \rightarrow 2$, $1 \rightarrow 3$ transitions are needed (see p. 426). The classical results show, contrary to expectations,* that the theoretical elastic cross-sections for p-H_2 can be as much as a factor of two smaller than those for o-H_2 in the rainbow region.[49] This result is also in agreement with the quantum calculations (see Table 2). The measured ratios presented in Table 2 are compared with those calculated for the different approximations in Figure 14. Considering the relatively large errors in these first experiments and the uncertainties in the theory, the overall agreement is quite gratifying.† In general, the classical results do not agree as well with experiment as the quantum-mechanical results, suggesting that the former are less reliable. This is hardly surprising in view of the assumptions made in applying classical mechanics to a scattering process with extreme quantum features, associated with the $j = 0$ and $j = 1$ rotational states – far from the correspondence limit – and the relatively widely spaced interference undulations in the angular distributions. As far as we are aware this is the most severe test of classical scattering theory in molecular collisions reported so far. The good performance of classical theory under unfavourable circumstances leads us to hope that with some refinements it may be able to compete with quantum mechanics in calculating inelastic cross-sections even under more extreme quantum-mechanical conditions. Parallel studies in electron–atom scattering at higher energies[54] also have recently shown classical mechanics to be valid over a much wider range than previously thought possible. Aside from its conceptual

* Since the rotational period of a $j = 1$ molecule ($\tau_{rot} = 3 \times 10^{-13}$ s) is still considerably longer than the time for a collision $\left(t = \frac{3\,\text{Å}}{\text{relative vel.}} \simeq 1.5 \times 10^{-14}\,\text{s}\right)$, we had anticipated that both the $0 \rightarrow 0$ and $1 \rightarrow 1$ cross-sections would be the same.

† The only apparently serious discrepancy is for p-H_2 at $\Theta = 32°$. Since these cross-section ratios were extracted from the valley of spectra of the type shown in Figures 8 and 9 it is conceivable that the experimental errors are greater than those estimated and shown in Figure 14.

[53] D. G. Truhlar, *J. Chem. Phys.*, 1973, **58**, 3109.

[54] A. Burgess and I. C. Percival, *Adv. Atom. Mol. Phys.*, 1968, **4**, 109.

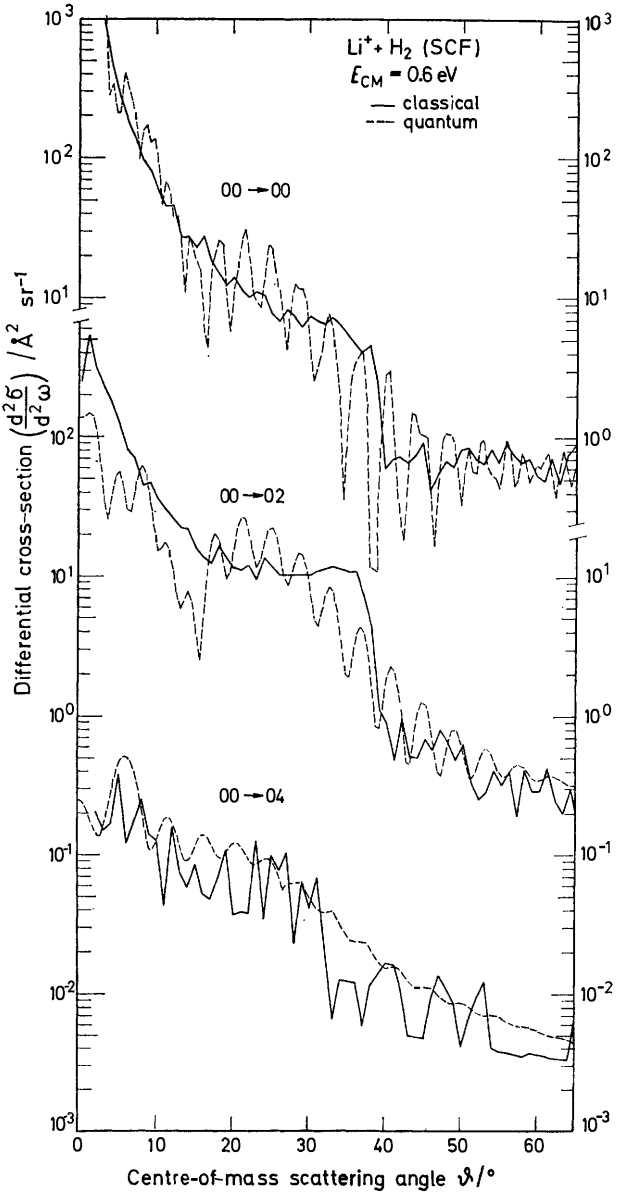

Figure 13 *Comparison of theoretical calculated differential cross-sections for elastic* $j = 0 \rightarrow 0$ *and inelastic* $j = 0 \rightarrow 2$ *and* $j = 0 \rightarrow 4$ *scattering of* Li^+–p-H_2 *at* $E_{cm} =$ 0.6 eV. *The dashed curves have been calculated for the Lester hypersurface using quantum-mechanical scattering theory with a converged basis set.*[45] *The solid-line curves have been calculated using classical mechanics, with an angular bin width of* 1°.[49]

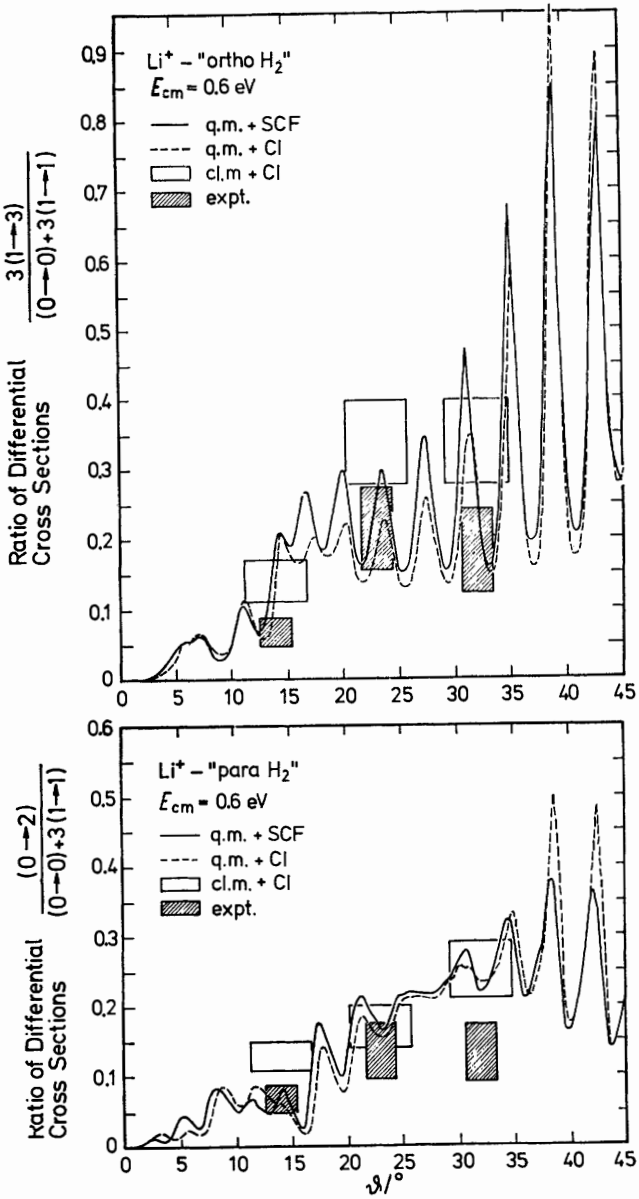

Figure 14 *Comparison of measured relative cross-sections for the $j = 0 \rightarrow 2$ (top diagram) and for the $j = 1 \rightarrow 3$ transitions (bottom diagram) with theoretical values for the SCF and CI potential hypersurfaces. The shaded boxes show the experimental values with their estimated errors. The open boxes are the classical results with the Monte Carlo angular bin widths and estimated standard deviations.*[49] *The quantum-mechanical results were taken from ref.* 51*d*

simplicity, classical theory has the big advantage that the computations are more than an order of magnitude faster than with quantum theory.

B. Vibrational Excitation.—As pointed out in connection with Figure 3, vibrational excitation is caused by collision-induced forces along the intramolecular axis of the molecule. Figure 15 shows the appropriate projections of the potential hypersurface. For simplicity the orientation angle γ has been fixed at the two orientations $\gamma = 0°$ and $\gamma = 90°$, corresponding to collinear and perpendicular collisions, respectively. Thus the potential energy is plotted as a function of the Li^+–H_2 distance R and the intramolecular distance r. For some fixed large R the potential curve is essentially the Morse-type curve of the free H_2 molecule. As R is diminished, the intermolecular repulsion between the Li^+ and the H_2 causes the $V(r)$ curves to be shifted upwards. Moreover, the curves become distorted, and for both orientations the minimum is shifted to smaller r values. This shift in minimum location is more clearly seen by considering the location of the minimum energy path, which is defined as the line of least potential energy, projected onto the (r, R)-plane as shown on the bottom portion of Figure 15.

In the usual picture in which additivity of repulsive atom–atom potentials is assumed one finds that the H_2 bond distance is contracted for $\gamma = 0$ and is expanded for 90°. In the latter case the incoming atom forces itself between the atoms of the molecule, thereby producing an expansion. Figure 15 shows that the actual behaviour is in agreement with the usual picture for $\gamma = 0$ but disagrees for $\gamma = 90°$. The anomalous contraction of the H_2 bond for $\gamma = 90°$ was first observed by Krauss and Mies[55] in their calculations of the He–H_2 potential hypersurface and was attributed to an increase in the electron density between the two protons, which tends to pull these together, as predicted by the Hellmann–Feynmann theorem.[56] Only at very small distances ($R < 1.00$ Å), not shown in Figure 15, do the atom–atom repulsion forces lead to an expansion of the H_2 bond.

Unfortunately, it is still not possible to carry out an accurate close-coupling quantum-mechanical calculation of vibrational excitation for comparison with the experiments.* The reason is that the computing time increases with the number of rotational states N approximately as N^6 where all of the energetically accessible states are included. Even if we were to neglect the vibrational states and include only open channels for p-H_2, we would need to include about 14 rotational states (196 channels) at $E_{cm} = 3.6$ eV, which would mean an increase in computing time over the rotational excitation problem at $E_{cm} = 0.6$ eV by a factor of ≈ 500. The classical calculations also take longer since the probability of backward scattering and vibrational excitation is much smaller than for rotational excitation, but they are possible and have been carried out.[49] To

* Converged close-coupling partial cross-sections for vibrational excitation have been computed at 1.2eV;[51d] 74 channels were needed. Nearly converged partial cross-sections have also been reported at 1.2 eV.[51a,c,d]

[55] M. Krauss and F. H. Mies, *J. Chem. Phys.*, 1965, **42**, 2703.

[56] J. O. Hirschfelder, C. F. Curtiss, and R. B. Bird, 'Molecular Theory of Gases and Liquids', Wiley, New York, 1954, p. 932.

simplify the classical calculations, account was taken of the fact that only the nearly central collisions (with small impact parameters) are responsible for the backward scattering observed in the experiments. Trial calculations were first performed to ascertain the actual range of impact parameters needed. Then a total of 2×10^4 trajectories were run for both the ortho and para molecules. To account approximately for apparatus smearing, each transition was assigned a triangular shape with a width in accord with the results of Figure 10. The classical results are shown in Figure 16, where the composite spectrum is compared with the experimental results by normalizing the calculated spectrum to the measured spectrum at the maximum.

The classical calculations show, in agreement with the preliminary interpretation presented in Section 2D, that rotational excitation is improbable in the backward direction. The comparison with experiment shows that the experimental inelastic transition probabilities are about a factor of two larger than theory. This is not surprising since the classical calculations do not take account of tunnelling beyond the steep potential barrier. As shown in Figure 14, the force on the oscillator (curvature of the reaction co-ordinate) increases markedly with decreasing R. Thus tunnelling could lead to a sizeable increase in the vibrational excitation probability.

4 Conclusions

The results presented here for Li^+–H_2 provide the first direct and detailed test of the theories used in calculating inelastic differential collision cross-sections. Thus the theoretical steps given in Figure 1, starting with the Hamilton operator at the upper left, yield results which, within the limits given in Figure 14, are in reasonable agreement with experiment. Additional experimental and theoretical work is needed to show whether the remaining differences are real, and if so if they can be attributed to inaccuracies in either the theory (potential hypersurface or scattering cross-section) or experiment. Clearly, the next step is to seek ways to 'invert' the cross-section data in order to be able to measure the important parts of the hypersurface. In this way, it will also be possible for the quantum chemist to know which parts of the hypersurface are most important and need to be calculated with the greatest accuracy for a given inelastic process. The quantum-mechanical trial and error procedure used routinely in elastic scattering to interpret experimental results does not appear feasible because of the excessive computing times. The near agreement of the pure classical cross-sections with experiment and quantum theory is, however, encouraging. A classical inversion of inelastic cross-sections now seems quite feasible.

The apparent success of classical mechanics in explaining our experiments does not, of course, imply that pure classical mechanics can always be used to calculate energy transfer under gas-kinetic conditions. Our experience has been that classical mechanics can be expected to perform well if the transition probabilities are large, say greater than 10^{-1}, and this is presently a necessary condition for the observability of an inelastic quantum transition in scattering experiments. At thermal energies the transition probabilities will be frequently

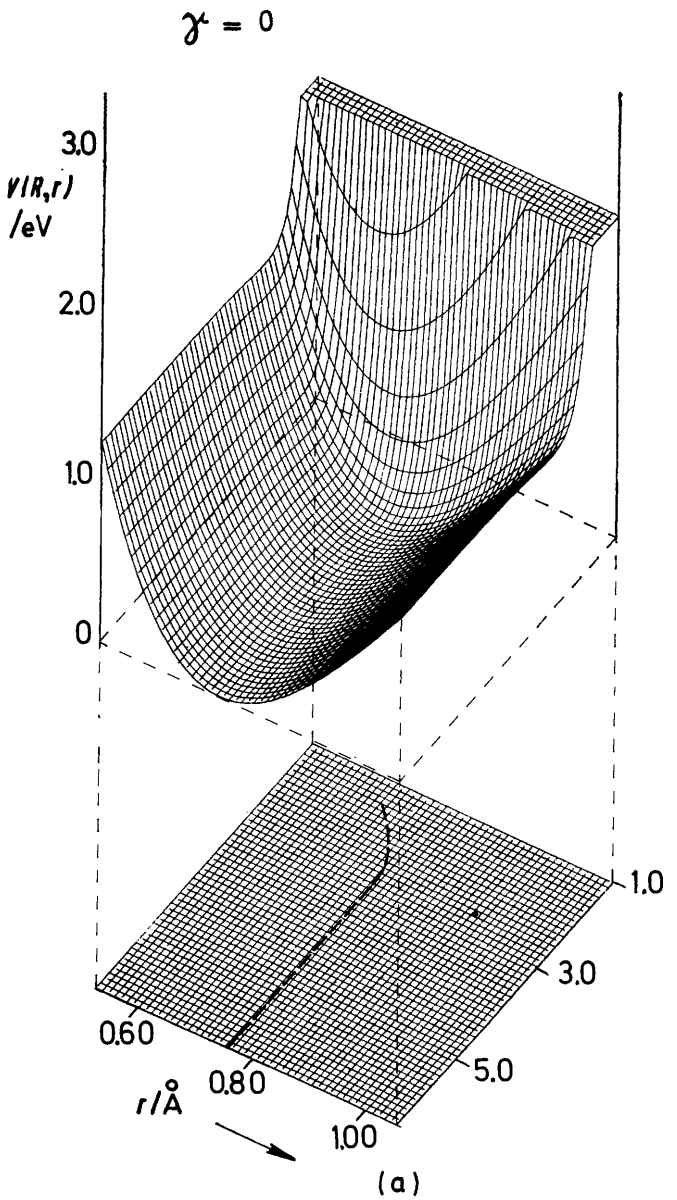

Figure 15 *The potential energy $V(R, r)$ for a Li^+ ion approaching a non-rotating H_2 molecule with $\gamma = 0°$ and $\gamma = 90°$ is plotted as a function of R and γ. For large R the r-dependent curves approach the Morse-type potential curves of a free H_2 molecule. With decreasing R the bond distance gets smaller, especially for the $\gamma = 0$ configuration. The dashed line in the r, R plane at the bottom of each hypersurface shows the projection of the reaction co-ordinate*

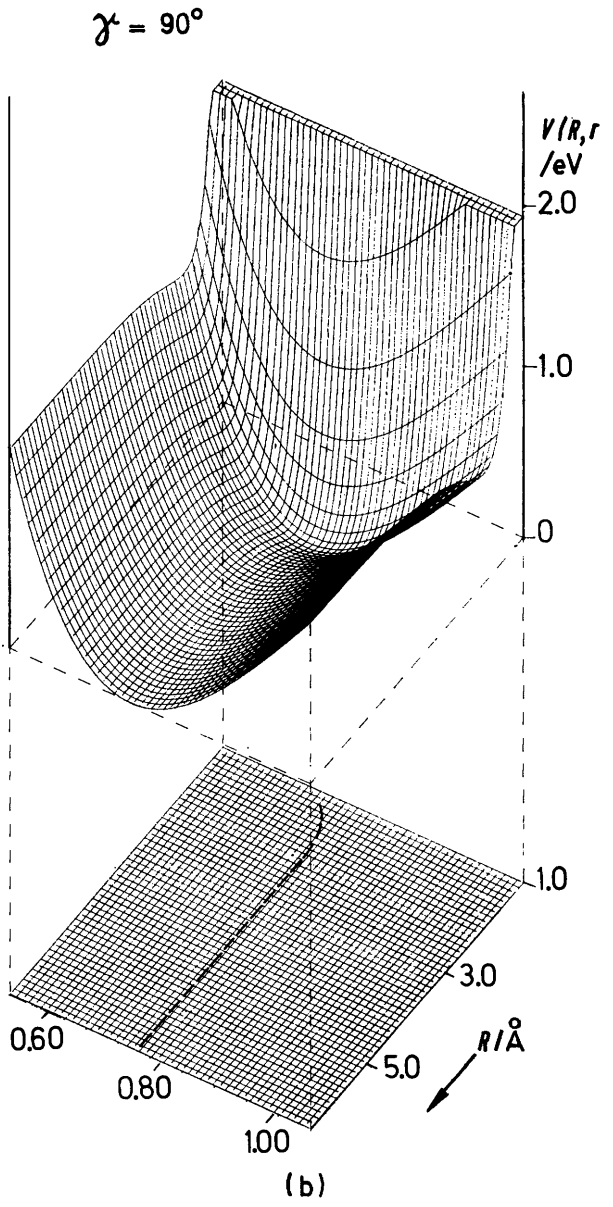
γ = 90°
V/R,r
/eV
2.0
1.0
0
1.0
3.0
5.0
R/Å
0.60
0.80
1.00
(b)

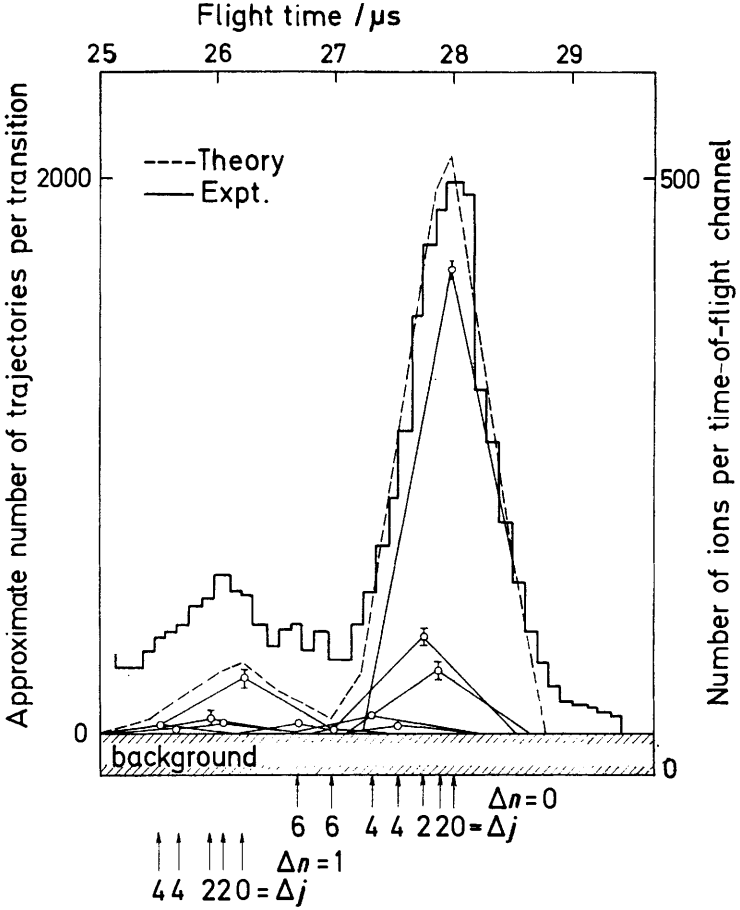

Figure 16 *Comparison of measured and* ab initio *classically calculated time-of-flight spectra for vibrational excitation* (E_{cm} = 3.6 eV, ϑ_{cm} = 167°). *The expected peak locations are shown at the bottom. The individual calculated contributions (solid lines) have been adjusted for ortho:para ratios of normal* H_2. *The dashed line shows the sum of the individual contributions*

much lower and more like those presented in Figure 2. An attempt using classical mechanics at reproducing the results of Figure 2 was quite unsuccessful.[57] Only rotational excitation cross-sections at $\vartheta > 90°$ were in fair agreement, whereas at $\vartheta < 90°$ the classical results were too small by many orders of magnitude. No vibrational excitation could be made to occur classically at energies below 4.00 eV. The inadequacy of classical mechanics indicates the

[57] G. D. Barg and J. P. Toennies, *Faraday Discuss. Chem. Soc.*, 1973, No. 55, p. 59.

importance of classically forbidden regions of the potential surface in energy transfer. Thus, under gas-kinetic conditions a semi-classical calculation similar to that used by Marcus,[58] Miller,[59] and others will be necessary.

In addition to providing an exacting test of theory, these scattering experiments point the way for future quantum-resolved studies of neutral–neutral inelastic collisions. Such experiments are now within reach for a large number of systems.

Many former students have contributed to our studies of Li^+–H_2, which were started ten years ago. I would like especially to thank J. Schöttler, W. D. Held, R. David, M. Faubel, H. Fremerey, and G.-D. Barg. Drs. H. van den Bergh, G. Kendall, and P. McGuire also made valuable contributions. I am grateful to W. A. Lester for communicating the results of Figure 14 prior to publication and for enlightening discussions and correspondence. I would also like to thank him, A. S. Dickinson, and my colleagues Barg, Kendall, and McGuire for reading and criticizing the manuscript. The initial support for this research was generously provided by the Deutsche Forschungsgemeinschaft.

[58] R. A. Marcus, *Faraday Discuss. Chem. Soc.*, 1973, No. 55, p. 34.
[59] W. H. Miller, *Adv. Chem. Phys.*, 1974, **25**, 63.